Chemical Science

ROYAL SOCIETY OF CHEMISTRY

EDGE ARTICLE

View Article Online
View Journal | View Issue

Cite this: *Chem. Sci.*, 2023, **14**, 10176

All publication charges for this article have been paid for by the Royal Society of Chemistry

Received 21st April 2023
Accepted 21st August 2023

DOI: 10.1039/d3sc02062b

rsc.li/chemical-science

Design rules for reciprocal coupling in chemically fueled assembly†

Xiaoyao Chen, ‡ Brigitte A. K. Kriebisch, ‡ Alexander M. Bergmann and Job Boekhoven *

Biology regulates the function and assembly of proteins through non-equilibrium reaction cycles. Reciprocally, the assembly of proteins can influence the reaction rates of these cycles. Such reciprocal coupling between assembly and reaction cycle is a prerequisite for behavior like dynamic instabilities, treadmilling, pattern formation, and oscillations between morphologies. While assemblies regulated by chemical reaction cycles gained traction, the concept of reciprocal coupling is under-explored. In this work, we provide two molecular design strategies to tweak the degree of reciprocal coupling between the assembly and reaction cycle. The strategies involve spacing the chemically active site away from the assembly or burying it into the assembly. We envision that design strategies facilitate the creation of reciprocally coupled and, by extension, dynamic supramolecular materials in the future.

Introduction

Biological supramolecular structures like the nucleolus, the transmembrane ATPases, and the cytoskeleton are tightly regulated using non-equilibrium chemical reaction cycles, giving them unique properties like the capacity to heal or form patterns.[1–3] These reaction cycles are catalytic and convert molecules with high chemical potential into their lower chemical potential counterparts, like the enzymatic conversion of ATP to ADP. Upon doing so, the enzyme is temporarily activated for a function like assembling. Prototypical examples are the ATP-driven formation of actin filaments or ATP-fueled ATPase pumps. *Vice versa*, the resulting assemblies also regulate the activation and deactivation of their building blocks.[4–6] Thus, the reaction cycle and assembly are reciprocally coupled (Scheme 1A). Again, actin assembly is a great example—ATP activates monomeric, globular actin (G-actin) for assembly into filaments.[4] Upon assembly, actin changes its conformation (F-actin), resulting in an increased ATP hydrolysis rate.[5] ATP hydrolysis triggers disassembly. Thus, the reaction cycle activates and deactivates molecules for assembly. *Vice versa*, the assembly affects the kinetics of the reaction cycle by catalyzing hydrolysis—the assembly process and its reaction cycle are reciprocally coupled. In an extreme case of reciprocal coupling, a building block's activation can only occur in the non-assembled state, and its deactivation can only occur in the assembled state.[7] In such a scenario, building blocks must assemble and disassemble to proceed through a reaction cycle. Such reciprocal coupling is a prerequisite for driven self-assembly and behavior like dynamic instabilities, treadmilling, pattern formation, and oscillations between morphologies. Even though reciprocal coupling is ubiquitous in biology, synthetic assemblies with similar dynamic behavior are underexplored. To create synthetic assemblies with similar dynamic behavior, we must understand mechanisms by which assembly and reaction cycle reciprocally affect each other. Moreover, we need design rules by which we can control the nature of feedback and the degree of reciprocal coupling interaction.

So far, several fuel-driven chemical reaction cycles have been developed—those that are driven by the oxidation of reducing agents and *vice versa*,[8–10] the hydration of high-energy reagents like carbodiimides,[11–13] the hydrolysis of methylating agents,[14] or biomolecules like adenosine triphosphate (ATP).[15,16] These chemical reaction cycles activate and deactivate molecules for assembly into, *e.g.*, micelles,[9,17,18] vesicles,[19] droplets,[12,20] colloids,[8,11] nano- or microparticle clusters,[21,22] and fibers.[11,14,16] Moreover, molecular assemblies that catalyze chemical reactions are well known and include micelles that catalyze Diels–Alder reactions,[23] membrane-less organelles catalyze aldol reactions,[24] catalytic fibers and nanotubes catalyze aldol reactions,[25] ester hydrolysis,[26,27] Diels–Alder reactions.[28] However, systems where the two concepts are combined, *i.e.*, a reaction cycle that regulates assembly and the assembly that regulates the reaction cycle, are underexplored.[10,11,17,29–31] Design rules are needed to control the nature of feedback and the degree of reciprocal coupling.

Department of Chemistry, School of Natural Sciences, Technical University of Munich, Lichtenbergstrasse 4, 85748 Garching bei München, Germany. E-mail: job.boekhoven@tum.de

† Electronic supplementary information (ESI) available: Materials and methods description and additional data on the characterization of precursor and product (ESI-MS, NMR, HPLC), a description of the used kinetic model and the observed and fitted rate constants, fluorescence spectroscopy data, Fourier-transform infrared spectroscopy data, kinetic data, confocal microscope images, titration data (PDF). See DOI: https://doi.org/10.1039/d3sc02062b

‡ X. C. and B. A. K. K. contributed equally.

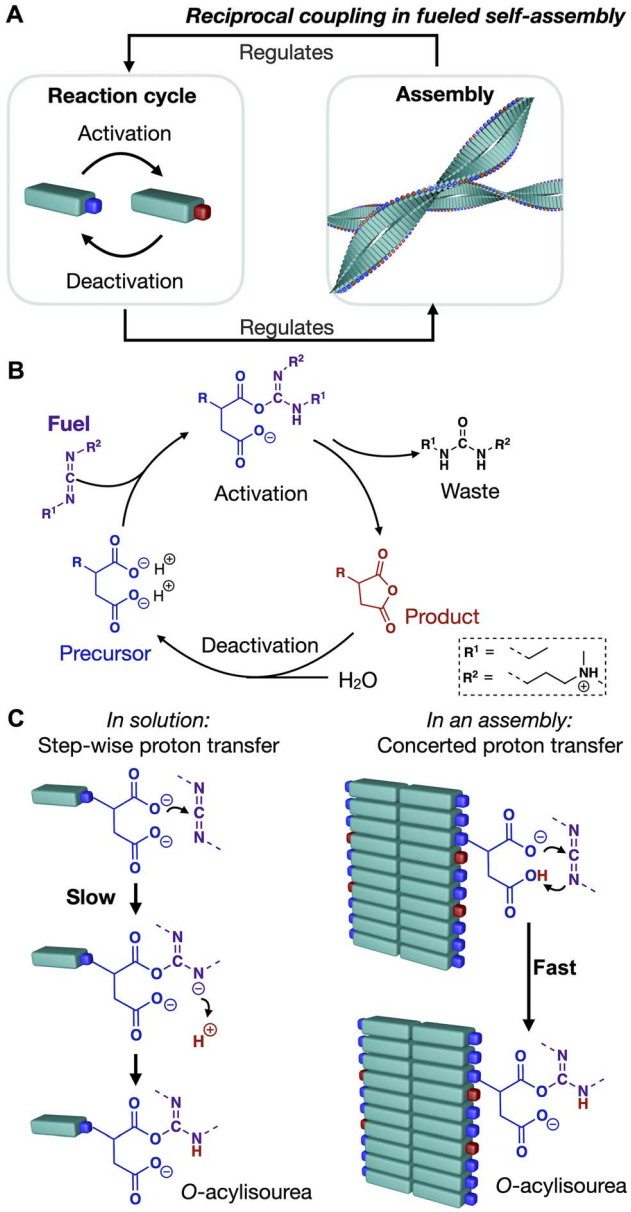

Scheme 1 A) Simplified scheme of reciprocal coupling in chemically fueled assemblies. The assembly is regulated by the reaction cycle and *vice versa*. (B) Chemically fueled reaction cycle. (C) Protonation of precursor controls activation reaction pathway: stepwise *vs.* concerted proton transfer.

We recently found a chemically fueled peptide that forms fibers that display reciprocal coupling between assembly and cycle (Scheme 1).[31] In the chemical reaction cycle, an anionic dicarboxylate peptide (precursor) converts into a non-charged anhydride (product) (Scheme 1B) by reacting with a carbodiimide. The hydrophobization, upon converting to an anhydride, induces self-assembly into fibers. Simultaneously, hydrolysis of the anhydride reinstates the negative charges on the precursor, which induces disassembly.[11] Reciprocally, we demonstrated that the assembly into fibers accelerates both the EDC-consuming activation of the peptide and the deactivation of the building block through hydrolysis (Scheme 1C).[31] The underlying mechanism has to do with the organization of the active sites of the peptide, which affects their apparent pK_a and thereby changes the reaction pathway. Peptides that do not assemble have a relatively low apparent pK_a and, thus, a low degree of protonation. Organizing the peptides into fibers increases the degree of protonation of the active sites, affecting whether the rate-determining step of the activation reaction proceeds *via* the slow stepwise or the fast concerted proton transfer pathway (Scheme 1C). Besides, the strength of hydrogen bonding also affects the deactivation rate. We hypothesized that the hydrogen bonding of a neighboring amide and the anhydride carbonyl's oxygen increases the carbonyl carbon's electrophilicity. Thereby, the anhydride hydrolysis is accelerated.

In this work, we demonstrate design strategies by which the degree of reciprocal coupling and its nature can be tuned (Fig. 1A). In one peptide, Ac–FAVD, the active site is attached to a non-assembling peptide (Fig. 1B). In one peptide design, Fmoc–AVG$_n$D, the active site is attached to a peptide that stacks into fibers. We space the chemical active site further from the peptide stack with a glycine spacer and an ethylene glycol spacer (Fig. 1C and D). Finally, we attach the active site to the self-assembling peptide but bury it inside the peptide stack and place it at a different position in the peptide sequence (Fig. 1E). We measure the reciprocal coupling between assembly and reaction kinetics for each design strategy.

Results and discussion

The degree of reciprocal coupling as a function of spacer length

The internal ordering or rigidity of the chemically fueled fibers results from stacking the hydrophobic Fmoc-group and β-sheet hydrogen bonds between the alanine and valine. To regulate the rigidity's effect on the apparent pK_a of the carboxylates, which are the active site, we spaced it away from the peptide domain responsible for the fiber's rigidity with a glycine linker. We designed the peptides Fmoc–AVG$_n$D–OH (G$_n$) with $n = 0, 1, 2, 3$, *i.e.*, G$_0$, G$_1$, G$_2$, G$_3$ (Fig. 1C). We chose glycine (G) as a flexible spacer because it lacks a side group, having the greatest freedom of rotation of the N–C$_\alpha$ (phi, φ) and C$_\alpha$–C′ (psi, ψ) and, thus, the lowest propensity to form β-sheets.[32,33] We dissolved the peptides G$_n$ at 2.5 mM in an aqueous buffer of 200 mM MES at pH 6. The addition of 50 mM 1-ethyl-3-(3-dimethylaminopropyl)carbodiimide (EDC) initiated the reaction cycle and led to the formation of a dense network of bundled fibers for all peptides (Fig. 2A). We determined the critical aggregation concentration of the peptides by a Nile red fluorescence assay. We used Nile red's increased emission intensity as a proxy for fiber formation. We added increasing amounts of peptide to a solution of 50 mM EDC and measured the fluorescence intensity (Fig. S1A–D†). The peptide needed to get the first evidence of assemblies was 0.5 mM. We then used the kinetic model (*vide infra*) to calculate the amount of anhydride around 0.2–0.3 mM when 0.5 mM precursor is used. Thus, we conclude that the anhydride's critical aggregation concentration (CAC) of the G$_n$ peptides is below 0.3 mM. We studied the kinetics of the reaction cycle for G$_n$ by applying fuel and

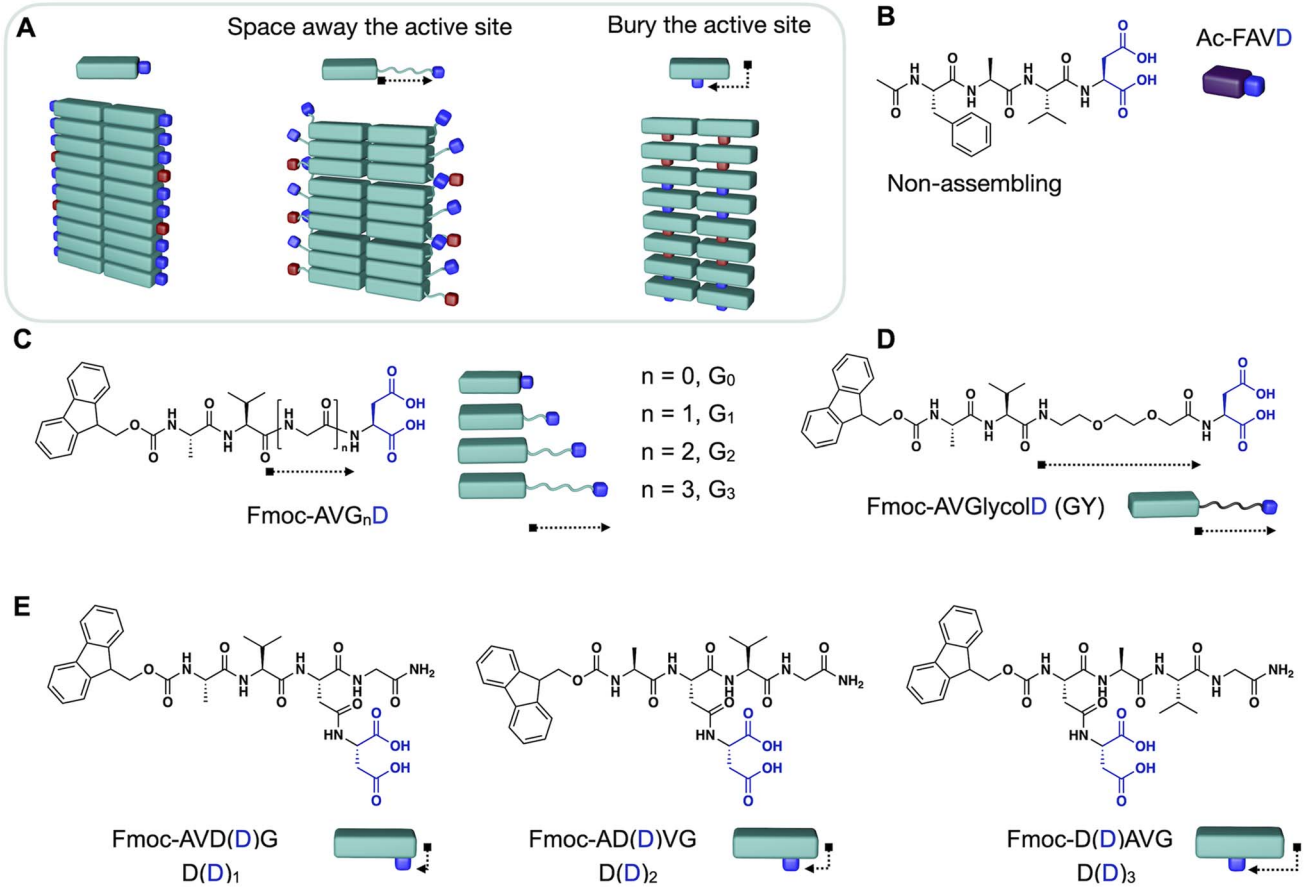

Fig. 1 Molecular design strategies to control reciprocal coupling and the nature of feedback. (A) Schematic representation of the design strategies. Either the active site is spaced away or buried in the stack compared to the original design (left). (B–E) Molecular design of precursor to regulate reciprocal coupling in chemically fueled assemblies. (B) The non-assembling compound as a reference. Spacing the aspartic acid away from the peptide core Fmoc–AV with (C) Gly-spacers and (D) an ethylene glycol segment. (E) Bury the aspartic acid in the peptide core by changing its position in the peptide sequence.

using a benzylamine quench[34] to stop the reaction cycle at predetermined time points. Benzylamine reacts with the anhydride (the activated peptide) to form the stable benzylamide, and the increase in pH stops the activation reaction. We monitored the concentration of fuel and benzylamide as a measure of the anhydride by high-performance liquid chromatography (HPLC) (Fig. 2B, C, S2A–C, G–I and S3–S7†). The activated peptide was temporarily sustained and decayed as the system ran out of fuel.

To quantify the nature of feedback and the degree of reciprocal coupling between the fibers and the reaction cycle, we used the non-assembling peptide Ac–FAVD–OH (Ac–FAVD, Ac = acetyl, F = phenylalanine) as a reference (Fig. S8A†). We observed that all G_n consumed EDC faster than Ac–FAVD (Fig. 2B, S2A–C and S3–S7†). Moreover, the anhydride of all G_n peptides was hydrolyzed faster than Ac–FAVD (Fig. 2C, S2G–I and S3–S7†). A kinetic model was used to fit the data and estimate all rate constants, confirming the acceleration (ESI – Kinetic model†).[11–13,35–37] The peptide without spacer G_0 showed the largest increase in the second-order rate constant of activation relative to Ac–FAVD, *i.e.*, a factor of 4.3 (Fig. 2D and Table S3†). In contrast, the acceleration of the activation decreased to 3.3/2.9/2.7 for G_1, G_2, G_3 compared to Ac–FAVD. Moreover, the rate constant of anhydride hydrolysis remained more or less constant with varying Gly spacer lengths and ranged between 2.1–2.2-fold acceleration compared to the non-assembling Ac–FAVD (Fig. 2D and Table S3†).

For the assembly to accelerate the activation, two conditions must be fulfilled.[31] First, the assembly is a co-assembly of activated and deactivated peptides, *i.e.*, precursors and anhydrides. Second, the apparent pK_a of the deactivated peptide is shifted in the assembly compared to in solution. Indeed, we found by ^{1}H-NMR spectroscopy that the deactivated peptide co-assembled into the fibers in all cases of G_n (Fig. 2E, S9A–C and S10†). Over the entire 90 minute chemical reaction cycle, most of the peptide was in the self-assembled state. Even though all the anhydride hydrolyzed back to its precursor after 90 minutes, the precursor stayed trapped inside the assembled fibers, indicating that the disassembly rate for all precursors is very slow. Because most of the peptide is in the assembly, we expect the co-assembled peptide to be reactivated inside the fiber. As the co-assembled peptide is exposed to a different microenvironment than in solution, we expect a change in the apparent pK_a of the active site and, thus, its reactivity.[38,39]

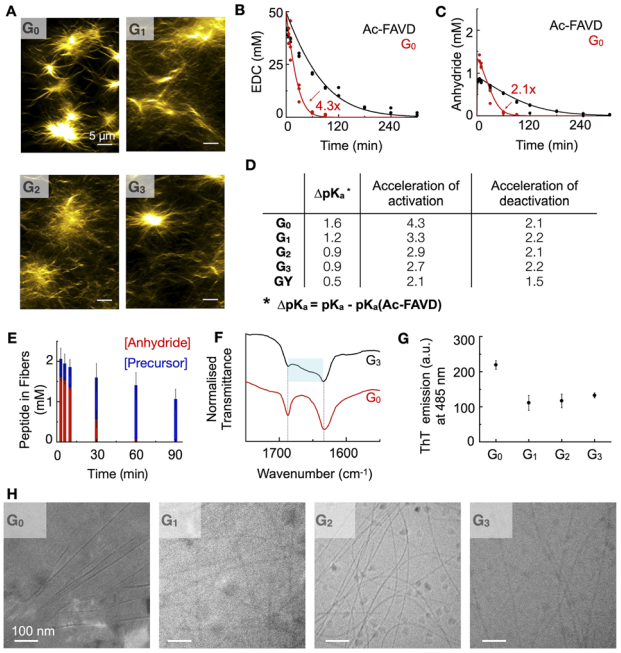

Fig. 2 The self-assembly and kinetic behavior of G_n and GY-peptide compared to Ac–FAVD. (A) Confocal micrographs of 2.5 mM G_n 10 minutes after fueling with 50 mM EDC. HPLC (markers) and kinetic model data (lines) as a function of time of (B) the EDC consumption for G_0 and Ac–FAVD, (C) the anhydride concentration of G_0 and Ac–FAVD after fueling with EDC, $n = 3$. (D) The influence of Gly's number and an ethylene glycol spacer (GY) on (1) the shift of apparent pK_a of G_n/GY to Ac–FAVD (2) the activation and deactivation reaction rate (k_1, k_4) of G_n/GY compared to Ac–FAVD. (E) The components of the chemically fueled fibers as a function of time determined by ^{1}H-NMR spectroscopy. Experiments were done in duplicate. (F) FT-IR spectra of G_0 and G_3 fueled with EDC at 3 min. Fmoc–OCNH band at 1687/1686 cm^{-1} and amide I band at 1633/1634 cm^{-1} (typical β-sheet). The blue box highlights the broad shoulder between 1640–1670 cm^{-1}. (G) Maximal ThT emission (a.u.) at 485 nm after excitation at 440 nm when 2.5 mM G_n is fueled with 10 mM EDC, $n = 3$. (H) Cryo-TEM micrographs of 2.5 mM G_n fueled with 25 mM EDC at 2 min. Scale bar 100 nm.

We determined the apparent pK_a by titration. We found that for the non-assembling Ac–FAVD, the apparent pK_a values were 4.2 and 2.2, which is in line with reference values for aspartic acid (Fig. S11A†).[40] In contrast, for all G_n, only a single apparent pK_a value was found with a shift to higher values, *i.e.*, 5.8 for G_0, 5.6 for G_1, 5.1 for G_2, and 5.1 for G_3 (Fig. S11B–E†).

Our combined findings conclude that the deactivated peptide is co-assembled with the activated peptide, and the change of its microenvironment compared to the non-assembled peptide changes the apparent pK_a of the active site. However, the further active site is spaced away from the fiber the smaller the change in apparent pK_a. As the activation reaction is rate limited by a proton transfer, shifting the apparent pK_a to a higher value increased the activation rate. Yet, the effect decreases with increasing glycine spacer. We hypothesize that more than two Gly-spacers do not lead to more conformational flexibility of the aspartic acid headgroup.

We studied the influence of the Gly spacers on the β-sheet interactions of the fibers by Fourier-Transform Infrared spectroscopy (FT-IR). With FT-IR measurements, the β-sheet interactions are normally characterized in a range of 1625–1640 cm^{-1}.[41] These fibers showed two predominant peaks: the amide I band at 1630 cm^{-1} (carbonyl stretch vibration responsible for the β-sheet interactions) and the Fmoc–OCNH band at 1690 cm^{-1} (Fig. 2F, S12A and B†). The amide I band is sensitive to hydrogen bonding in the assembly, and it broadens towards higher wavenumbers with increasing glycine spacer length. This broadening indicates that the peptide assemblies are less ordered, *i.e.*, the β-sheet interactions between peptides are decreased.[41] Moreover, we used a ThT assay to measure the assembly's ability to bind ThT, which is a measure of the flatness and, thus, the rigidity of the β-sheets of the assemblies.[42,43] The maximum emission intensity of ThT decreased by introducing Gly-spacers, indicating a decreased degree of β-sheet flatness and rigidity for G_n ($n = 1, 2, 3$) assemblies (Fig. 2G,

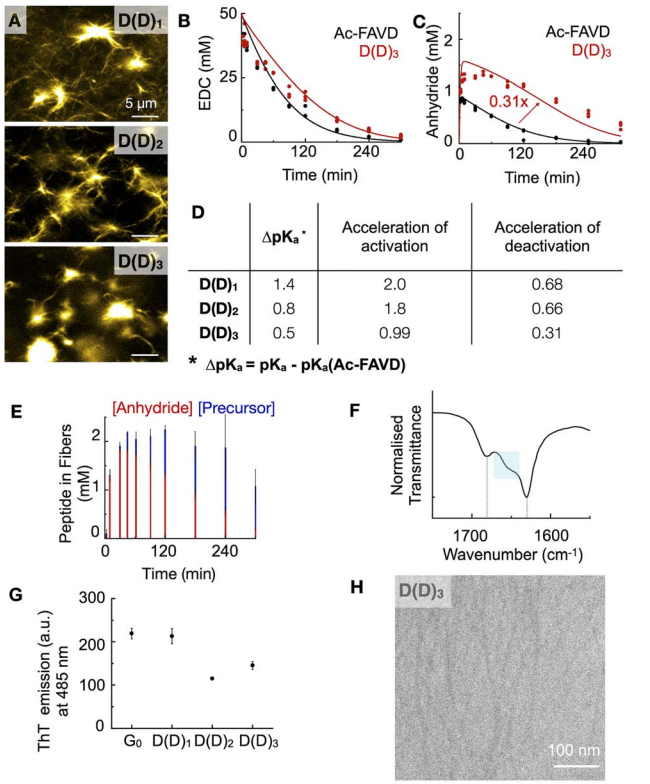

Fig. 3 The self-assembly and kinetic behaviour of D(D)$_n$ compared to Ac–FAVD. (A) Confocal micrographs of D(D)$_n$ 10 minutes after fueling with EDC. HPLC (markers) and kinetic model data (lines) as a function of time of (B) the EDC consumption for D(D)$_3$ and Ac–FAVD and (C) the anhydride concentration of Ac–FAVD and D(D)$_3$ after fueling with EDC $n = 3$. (D) The influence of the branched linker on (1) the shift of apparent pK_a of D(D)$_n$ to Ac–FAVD; (2) the activation and deactivation reaction rate (k_1, k_4) of D(D)$_n$ compared to Ac–FAVD. (E) The components of the chemically fueled fibers as a function of time determined by ^{1}H-NMR spectroscopy. Experiments were done in duplicate. (F) FT-IR spectra of D(D)$_3$ fueled with EDC at 3 min. Fmoc–OCNH band at 1681 cm^{-1} and amide I band at 1630 cm^{-1} (typical β-sheet). The blue box highlights the broad shoulder between 1640–1670 cm^{-1}. (G) Maximal ThT emission (a.u.) at 485 nm after excitation at 440 nm when 2.5 mM G$_0$/D(D)$_n$ is fueled with 10 mM EDC, $n = 3$. (H) Cryo-TEM micrographs of 2.5 mM D(D)$_3$ fueled with 25 mM EDC at 2 min. Scale bar 100 nm.

S13A–D and S14A–D†). Cryogenic-Transmission Electron Microscopy (Cryo-TEM) studies showed that G_0 assembled into broad tapes with a width of 52 ± 11 nm whereas G_n ($n = 1, 2, 3$) assembled into thin fibers with a width of 7 ± 2 nm (Fig. 2H). The planar tape structure of G_0 indicates that the active aspartic acid headgroup is conformationally more constrained than in the thin fiber assemblies of G_n ($n = 1, 2, 3$).

To further improve the flexibility of the spacer unit, we used an ethylene glycol spacer. We designed Fmoc–AV–ethylene glycol-D–OH, *i.e.*, GY (Fig. 1D). We added 50 mM EDC to 2.5 mM GY in MES buffer at pH 6 to initiate the reaction cycle, which led to the formation of fibers (Fig. S8B†). We determined the CAC to be around 0.2 mM (Fig. S1E†). The kinetic experiments showed that the activation was only 2.1-fold accelerated compared to Ac–FAVD. The anhydride hydrolysis rate constant was slightly by a 1.5-fold (Fig. 2D, Table S3, Fig. S2D, J, S4C, S7C and D†). Like G_n, ^{1}H-NMR spectroscopy showed that the deactivated peptide co-assembled into the GY fibers (Fig. S9D and S15†). In the fiber microenvironment, the apparent pK_a shifts to 4.7 (Fig. S11F†). Thus, compared to G_n, the pK_a-shift is lower, resulting in a lower acceleration of activation and deactivation. The FT-IR-spectra of GY showed next to the characteristic amide I band at 1630 cm^{-1} also a broad shoulder between 1640–1670 cm^{-1} (Fig. S12C†). This peak shape points to a random coil (1640–1650 cm^{-1}) next to elements of β-sheet structures (1625–1640 cm^{-1}), meaning that parts of the peptide assemblies are even less ordered than the G_n peptides.[41]

We conclude that introducing Gly-spacers as well as an ethylene glycol-spacer between the peptide core Fmoc–AV and the active site introduces conformational flexibility of the active aspartic acid headgroup and thus decreases the shift in the apparent pK_a value of the carboxylates. This enables us to tune the acceleration of the activation reaction compared to G_0. The higher the flexibility of the Gly *vs.* ethylene glycol, the greater the effect on the conformational flexibility of the active aspartic acid headgroup. The effect decreases and flattens if we introduce more than one Gly-spacer.

Tuning the reciprocal coupling by burying the active site

We designed the peptides Fmoc–AVD(D)G–NH_2 ($D(D)_1$), Fmoc–AD(D)VG–NH_2 ($D(D)_2$), and Fmoc–D(D)AVG–NH_2 ($D(D)_3$) in which the active site, *i.e.*, the aspartic acid, is placed at different positions in the Fmoc–AVG peptide sequence *via* an aspartic acid linker (Fig. 1E). Thus, the active site is branched away from the peptide chain and buried deeper into the fiber's core with increasing number. We hypothesize that the buried and branched dicarboxylate group disrupts the strong π–π interactions of the Fmoc-group and the β-sheet hydrogen-bonding interactions of the AV segment, thereby influencing the degree of reciprocal coupling. We dissolved 2.5 mM $D(D)_n$ in MES buffer at pH 6 and added 50 mM EDC to initiate the reaction cycle, which led to the formation of fibers (Fig. 3A). We found the CAC of these peptides to be below 0.3 mM (Fig. S1F–H†).

We analyzed the evolution of the $D(D)_n$ reaction cycle by HPLC and compared it to the non-assembling Ac–FAVD (Fig. 3B, C, S2E, F, K, L and S16–S18†). The data from our kinetic model showed that the activation rate constant was 2-fold to 1.8-fold accelerated for $D(D)_1$ and $D(D)_2$ but not accelerated for $D(D)_3$ compared to Ac–FAVD (Fig. 3B, D, S2E, F and S16–S18†). ^{1}H-NMR spectroscopy combined with HPLC

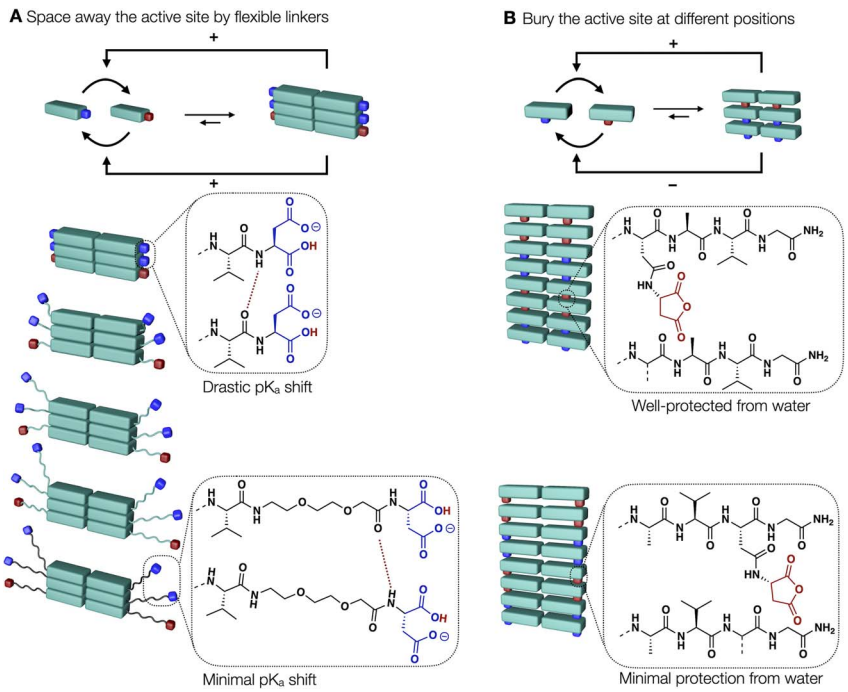

Fig. 4 Simplified scheme of molecular design tailoring the nature of feedback and the reciprocal coupling strength between assembly and reaction cycle. (A) Strategy of spacing away the active site. (B) Strategy of burying the active site.

showed that over the entire reaction cycle, the $D(D)_n$ fibers were a co-assembly of activated and deactivated peptides (Fig. 3E, S9E, F and S19†). As for the G_n and GY peptides, most of the peptide is trapped inside the assembly, indicating a slow disassembly rate. Thus, we expect the co-assembled $D(D)_n$ peptide to be reactivated inside the fiber as well. In the fiber microenvironment, the apparent pK_a changes, and thus the reactivity of the $D(D)_n$ peptides changes. The apparent pK_a we measured for $D(D)_n$ in its assembled state is and 5.6 for $D(D)_1$, 5.0 for $D(D)_2$ and 4.7 for $D(D)_3$ (Fig. S11G–I†). Thus, compared to the non-assembling Ac–FAVD, the apparent pK_a shifts 0.5–1.4 units higher (Fig. 3D). The further the branched active aspartic acid is spaced away from the Fmoc–fiber core, the less buried the active site is and the higher the apparent pK_a shift, and thus the greater acceleration of the activation reaction. Indeed, the acceleration of the activation reaction for $D(D)_n$ decreased from 2.0 to 0.99 from $D(D)_1$ to $D(D)_3$. In stark contrast to the G_n peptide series and the GY peptide, we found that the rate constant for activated $D(D)_n$ deactivation around 30% slower for $D(D)_1$ and $D(D)_2$ and 70% slower for $D(D)_3$, respectively than for Ac–FAVD (Fig. 3C, D, S2K, L and S16–S18†). We hypothesize that the hydrophobic fiber core excludes water. Thus, the buried anhydride, especially in $D(D)_3$, is protected from hydrolysis. In $D(D)_1$ and $D(D)_2$ fibers, the active site is less buried, and thus the anhydride is less protected from hydrolysis. This is in line with confocal microscopy that shows a dense fiber network for $D(D)_1$ and $D(D)_2$ while for $D(D)_3$ we observe more nucleation sites from which fibers grow (Fig. 3A).

In the FTIR-spectra, the $D(D)_3$ amide I band peaked at 1633 cm^{-1} and showed a broad shoulder between 1640–1670 cm^{-1} (Fig. 3F). This peak shape points to the presence of β-sheet structures (1625–1640 cm^{-1}) next to elements of a random coil (1640–1650 cm^{-1}), meaning that parts of the peptide assemblies are less ordered.[41] Going from $D(D)_1$ to $D(D)_3$, the broad shoulder increases, indicating less-ordered assemblies (Fig. 3F, S12D and E†). The maximum emission intensity of ThT for $D(D)_1$ is almost equal to G_0 as the aspartic acid branch does not disrupt the Fmoc-π–π interactions and the hydrogen-bonding interactions of alanine and valine. However, for $D(D)_n$ ($n = 2, 3$) assemblies, the signal was lower than G_0. In $D(D)_2$ the aspartic acid branch is placed between alanine and valine and we hypothesize it disrupts the hydrogen bonding. In $D(D)_3$, the aspartic acid branch disrupts the β-sheet hydrogen-bonding interactions of the AV-segment and the Fmoc-π–π interactions (Fig. 3G, S13A, E–G, S14A and E–G†). Cryo-TEM shows that $D(D)_3$ assembled into thin fibers with a width of 6 ± 1 nm (Fig. 3H). The combined dataset of FT-IR, ThT, and Cryo-TEM reveals weaker intermolecular interaction of $D(D)_n$ compared to G_0 (FT-IR), yielding less rigid assemblies. Moreover, the more the branched active aspartic acid is placed in the fiber core, $D(D)_1$ *vs.* $D(D)_3$, the less rigid are the assemblies. These findings corroborate our hypothesis that the buried dicarboxylate disrupts the strong π–π interactions of the Fmoc-group and the β-sheet hydrogen-bonding interactions of the peptide sequence AVG.

Molecular design tunes the nature and degree of reciprocal coupling

We establish the following design rules to regulate the reciprocal coupling between assembly and cycle. Molecular designs that yield high internal order in the assembly carried over to the active sites result in pK_a shift which changes the kinetics of the activation. This organization also yields a higher deactivation (Fig. 4). Spacing the active site away from the ordered assembly with a flexible linker decreases the effect (Fig. 4 and 2). Moreover, molecular designs in which the active site is buried in the hydrophobic fiber core, excludes it from water, and thus protects it from hydrolysis resulting in a strong deceleration of the deactivation reaction (Fig. 4 and 3).

Conclusions

We studied two molecular design strategies to tune the nature of feedback and the degree of reciprocal coupling between the assembly and reaction cycle in chemically fueled peptide assemblies (fibers). The reciprocal coupling couples to the internal structure, *i.e.* the rigidity of the peptide assembly, which we can tune with molecular design. We show that we can tune the propensity of the peptide to form β-sheet hydrogen bonding by spacing the chemically active site away from the peptide core or burying it in the peptide core responsible for the fiber rigidity. These design strategies enable us to tune the degree and nature of feedback. Thus, our findings allow us to establish heuristic design rules for controlling the degree and nature of reciprocal feedback. We envision that these design rules can be exploited in future work to create synthetic assemblies with kinetic asymmetry and tunable dynamic behavior like pattern formation, oscillations in morphology, and motility, as seen in living systems.

Data availability

The data supporting this study's findings are available from the corresponding author upon reasonable request.

Author contributions

J. B., B. A. K. K., and X. C. conceived the research and wrote the manuscript. J. B., B. A. K. K., and X. C. designed the experiments and analyzed the data. A. M. B. performed Cryo-TEM measurements.

Conflicts of interest

The authors declare no competing financial interest.

Acknowledgements

The BoekhovenLab is grateful for funding from the Deutsche Forschungsgemeinschaft (DFG, German Research Foundation) – Project-ID 364653263 – TRR 235, the European Research Council (ERC starting grant 852187), and the TUM Innovation Network – RISE funded through the Excellence Strategy. This research was

conducted within the Max Planck School Matter to Life, supported by the German Federal Ministry of Education and Research (BMBF) in collaboration with the Max Planck Society. X. C. is grateful for the financial support from the China Scholarship Council. B. A. K. K. is grateful for a Kekulé-Stipendium by the Verbandes der Chemischen Industrie. We are grateful for using the TEM infrastructure of the Dietz Lab and the TUM EM Core Facility. We thank Dr Héctor Soria-Carrera for his assistance with the figures.

References

1 C. Toyoshima, Structural aspects of ion pumping by Ca2+-ATPase of sarcoplasmic reticulum, *Arch. Biochem. Biophys.*, 2008, **476**, 3–11.
2 M. Dogterom and G. H. Koenderink, Actin-microtubule crosstalk in cell biology, *Nat. Rev. Mol. Cell Biol.*, 2019, **20**, 38–54.
3 I. Grummt, Life on a planet of its own: regulation of RNA polymerase I transcription in the nucleolus, *Genes Dev.*, 2003, **17**, 1691–1702.
4 W. Kabsch, H. G. Mannherz, D. Suck, E. F. Pai and K. C. Holmes, Atomic structure of the actin: DNase I complex, *Nature*, 1990, **347**, 37–44.
5 H. H. Katkar, A. Davtyan, A. E. P. Durumeric, G. M. Hocky, A. C. Schramm, E. M. De La Cruz and G. A. Voth, Insights into the Cooperative Nature of ATP Hydrolysis in Actin Filaments, *Biophys. J.*, 2018, **115**, 1589–1602.
6 G. J. Brouhard and L. M. Rice, Microtubule dynamics: an interplay of biochemistry and mechanics, *Nat. Rev. Mol. Cell Biol.*, 2018, **19**, 451–463.
7 G. Ragazzon and L. J. Prins, Energy consumption in chemical fuel-driven self-assembly, *Nat. Nanotechnol.*, 2018, **13**, 882–889.
8 J. Leira-Iglesias, A. Tassoni, T. Adachi, M. Stich and T. M. Hermans, Oscillations, travelling fronts and patterns in a supramolecular system, *Nat. Nanotechnol.*, 2018, **13**, 1021–1027.
9 S. M. Morrow, I. Colomer and S. P. Fletcher, A chemically fuelled self-replicator, *Nat. Commun.*, 2019, **10**, 1011.
10 J. Ottelé, A. S. Hussain, C. Mayer and S. Otto, Chance emergence of catalytic activity and promiscuity in a self-replicator, *Nat. Catal.*, 2020, **3**, 547–553.
11 M. Tena-Solsona, B. Rieß, R. K. Grötsch, F. C. Löhrer, C. Wanzke, B. Käsdorf, A. R. Bausch, P. Müller-Buschbaum, O. Lieleg and J. Boekhoven, Non-equilibrium dissipative supramolecular materials with a tunable lifetime, *Nat. Commun.*, 2017, **8**, 15895.
12 M. Tena-Solsona, C. Wanzke, B. Riess, A. R. Bausch and J. Boekhoven, Self-selection of dissipative assemblies driven by primitive chemical reaction networks, *Nat. Commun.*, 2018, **9**, 2044.
13 B. Rieß, C. Wanzke, M. Tena-Solsona, R. K. Grötsch, C. Maity and J. Boekhoven, Dissipative assemblies that inhibit their deactivation, *Soft Matter*, 2018, **14**, 4852–4859.
14 J. Boekhoven, W. E. Hendriksen, G. J. Koper, R. Eelkema and J. H. van Esch, Transient assembly of active materials fueled by a chemical reaction, *Science*, 2015, **349**, 1075–1079.
15 S. Maiti, I. Fortunati, C. Ferrante, P. Scrimin and L. J. Prins, Dissipative self-assembly of vesicular nanoreactors, *Nat. Chem.*, 2016, **8**, 725–731.
16 A. Sorrenti, J. Leira-Iglesias, A. Sato and T. M. Hermans, Non-equilibrium steady states in supramolecular polymerization, *Nat. Commun.*, 2017, **8**, 15899.
17 I. Colomer, S. M. Morrow and S. P. Fletcher, A transient self-assembling self-replicator, *Nat. Commun.*, 2018, **9**, 2239.
18 I. Colomer, A. Borissov and S. P. Fletcher, Selection from a pool of self-assembling lipid replicators, *Nat. Commun.*, 2020, **11**, 176.
19 C. Wanzke, A. Jussupow, F. Kohler, H. Dietz, V. R. I. Kaila and J. Boekhoven, Dynamic Vesicles Formed By Dissipative Self-Assembly, *ChemSystemsChem*, 2020, **2**, e1900044.
20 C. Donau, F. Späth, M. Sosson, B. A. K. Kriebisch, F. Schnitter, M. Tena-Solsona, H.-S. Kang, E. Salibi, M. Sattler, H. Mutschler and J. Boekhoven, Active coacervate droplets as a model for membraneless organelles and protocells, *Nat. Commun.*, 2020, **11**, 5167.
21 R. K. Grötsch, A. Angı, Y. G. Mideksa, C. Wanzke, M. Tena-Solsona, M. J. Feige, B. Rieger and J. Boekhoven, Dissipative Self-Assembly of Photoluminescent Silicon Nanocrystals, *Angew. Chem., Int. Ed.*, 2018, **57**, 14608–14612.
22 R. K. Grötsch, C. Wanzke, M. Speckbacher, A. Angı, B. Rieger and J. Boekhoven, Pathway Dependence in the Fuel-Driven Dissipative Self-Assembly of Nanoparticles, *J. Am. Chem. Soc.*, 2019, **141**, 9872–9878.
23 M. A. Würbser, P. S. Schwarz, J. Heckel, A. M. Bergmann, A. Walther and J. Boekhoven, Chemically Fueled Block Copolymer Self-Assembly into Transient Nanoreactors, *ChemSystemsChem*, 2021, **3**, e2100015.
24 M. Abbas, W. P. Lipinski, K. K. Nakashima, W. T. S. Huck and E. Spruijt, A short peptide synthon for liquid-liquid phase separation, *Nat. Chem.*, 2021, **13**, 1046–1054.
25 C. Berdugo, J. F. Miravet and B. Escuder, Substrate selective catalytic molecular hydrogels: the role of the hydrophobic effect, *Chem. Commun.*, 2013, **49**, 10608–10610.
26 C. Zhang, X. Xue, Q. Luo, Y. Li, K. Yang, X. Zhuang, Y. Jiang, J. Zhang, J. Liu, G. Zou and X. J. Liang, Self-assembled peptide nanofibers designed as biological enzymes for catalyzing ester hydrolysis, *ACS Nano*, 2014, **8**, 11715–11723.
27 Z. Huang, S. Guan, Y. Wang, G. Shi, L. Cao, Y. Gao, Z. Dong, J. Xu, Q. Luo and J. Liu, Self-assembly of amphiphilic peptides into bio-functionalized nanotubes: a novel hydrolase model, *J. Mater. Chem. B*, 2013, **1**, 2297–2304.
28 Q. Jin, L. Zhang, H. Cao, T. Wang, X. Zhu, J. Jiang and M. Liu, Self-assembly of copper(II) ion-mediated nanotube and its supramolecular chiral catalytic behavior, *Langmuir*, 2011, **27**, 13847–13853.
29 C. Bonfio, C. Caumes, C. D. Duffy, B. H. Patel, C. Percivalle, M. Tsanakopoulou and J. D. Sutherland, Length-Selective Synthesis of Acylglycerol-Phosphates through Energy-Dissipative Cycling, *J. Am. Chem. Soc.*, 2019, **141**, 3934–3939.
30 S. Bal, K. Das, S. Ahmed and D. Das, Chemically Fueled Dissipative Self-Assembly that Exploits Cooperative Catalysis, *Angew. Chem., Int. Ed.*, 2019, **58**, 244–247.

31 B. A. K. Kriebisch, A. Jussupow, A. M. Bergmann, F. Kohler, H. Dietz, V. R. I. Kaila and J. Boekhoven, Reciprocal Coupling in Chemically Fueled Assembly: A Reaction Cycle Regulates Self-Assembly and Vice Versa, *J. Am. Chem. Soc.*, 2020, **142**, 20837–20844.
32 C. Ramakrishnan and G. N. Ramachandran, Stereochemical criteria for polypeptide and protein chain conformations. II. Allowed conformations for a pair of peptide units, *Biophys. J.*, 1965, **5**, 909–933.
33 P. Chakrabarti and D. Pal, The interrelationships of side-chain and main-chain conformations in proteins, *Prog. Biophys. Mol. Biol.*, 2001, **76**, 1–102.
34 F. Schnitter and J. Boekhoven, A Method to Quench Carbodiimide-Fueled Self-Assembly, *ChemSystemsChem*, 2021, **3**, e2000037.
35 L. S. Kariyawasam and C. S. Hartley, Dissipative Assembly of Aqueous Carboxylic Acid Anhydrides Fueled by Carbodiimides, *J. Am. Chem. Soc.*, 2017, **139**, 11949–11955.
36 X. Chen, M. Stasi, J. Rodon-Fores, P. F. Grossmann, A. M. Bergmann, K. Dai, M. Tena-Solsona, B. Rieger and J. Boekhoven, A Carbodiimide-Fueled Reaction Cycle That Forms Transient 5(4H)-Oxazolones, *J. Am. Chem. Soc.*, 2023, **145**, 6880–6887.
37 X. Chen, H. Soria-Carrera, O. Zozulia and J. Boekhoven, Suppressing catalyst poisoning in the carbodiimide-fueled reaction cycle, *ChemRxiv*, 2023, preprint, DOI: **10.26434/chemrxiv-2023-v8v53**.
38 T. K. Harris and G. J. Turner, Structural Basis of Perturbed pKa Values of Catalytic Groups in Enzyme Active Sites, *IUBMB Life*, 2002, **53**, 85–98.
39 C. Tang, A. M. Smith, R. F. Collins, R. V. Ulijn and A. Saiani, Fmoc-Diphenylalanine Self-Assembly Mechanism Induces Apparent pKa Shifts, *Langmuir*, 2009, **25**, 9447–9453.
40 *CRC Handbook of Chemistry and Physics*, ed. W. M. Haynes, CRC Press, Boca Raton, 95th edn, 2014.
41 G. Cheng, V. Castelletto, C. M. Moulton, G. E. Newby and I. W. Hamley, Hydrogelation and Self-Assembly of Fmoc-Tripeptides: Unexpected Influence of Sequence on Self-Assembled Fibril Structure, and Hydrogel Modulus and Anisotropy, *Langmuir*, 2010, **26**, 4990–4998.
42 J. S. Richardson and D. C. Richardson, Natural β-sheet proteins use negative design to avoid edge-to-edge aggregation, *Proc. Natl. Acad. Sci. U. S. A.*, 2002, **99**, 2754–2759.
43 V. I. Stsiapura, A. A. Maskevich, V. A. Kuzmitsky, K. K. Turoverov and I. M. Kuznetsova, Computational Study of Thioflavin T Torsional Relaxation in the Excited State, *J. Phys. Chem. A*, 2007, **111**, 4829–4835.